CHAPTER 3

WAVELETS AND MULTISCALE ANALYSIS

****

Over the last two decades, application of wavelet transform has been the focus of interest in several fields of science and engineering. Particularly, numerical analysis with wavelet received attention by mathematician and engineers. Wavelet analysis is a new approach called 'numerical microscope' in the areas of data compression, image processing, and time series analysis. Multiresolution property and various basis functions of wavelets have potential to solve PDEs, efficiently.

This chapter provides the fundamental background in the theory of wavelets and introduces wavelet based FEM as a simulation tool for wave propagation problem. The focus is on biorthogonal and orthogonal wavelets and also on multiscale method. The purpose of this chapter is to establish an improved framework for simulation of linear and nonlinear elastic wave propagation and guided wave based damage identification techniques feasible in the context of on-line SHM. The chapter is divided into two major sections: one for fundamentals background and theory of wavelets. The second section is devoted to multiscale analysis and numerical simulation of elastic waves in plate-like structure.

3.1 Literature Review of Wavelets

3.1.1 History of wavelets

The first mention of the wavelet analysis appears to be in the dissertation of Alfred

Haar (1910), titled “On the theory of the orthogonal function systems.” His research on orthogonal systems of functions led to the development of a set of rectangular basis functions. Little advancement in the field of wavelets was reported after Haar’s work, until a physicist, Paul Levy, investigated the Brownian motion in the 1930s. He discovered that the scale-varying function, that is, the Haar basis function, was better suited than the Fourier basis functions for studying subtle details in the Brownian motion. In addition, the Haar basis function can be scaled into different intervals, therefore providing higher precision when modeling a function than that provided by the Fourier basis function. Several individuals, such as John Littlewood, Richard Paley, Elias M. Stein, and Norman H. Ricker have contributed, from 1930s to 1970s. In 1982 Jean Morlet a French geophysicist introduced the concept of a ‘wavelet’. Morlet has developed and implemented the technique of scaling and shifting of the analysis window functions in analyzing acoustic echoes. This study marked the beginning of the era of wavelet research. Alex Grossmann, theoretical physicist, studied inverse formula for the wavelet transform. The joint collaboration of Morlet and Grossmann yielded a detailed mathematical formulation of the continuous wavelet transforms and their various applications, of course without the realization that similar results had already been obtained in 1950's by Calderon, Littlewood, Paley, and Franklin. This rediscovery of the old concepts provided a new method for decomposing a function or a signal. Following up the impactful work of Morlet and Grossmann, numerous researchers have invested significant effort in further developing the theory of wavelet transform. Many eminent mathematicians e.g. I. Daubechies, A. Grossmann, S. Mallat, Y. Meyer, R. A. deVore, R. Coifman, V. Wickerhauser made a remarkable contribution to the wavelet theory.

Perhaps the most important step that has led to the prosperity of the wavelets was

the invention of multiresolution analysis by Meyer (1987) and Mallat (1989). Such an invention was introduced by a paper written by Meyer on orthogonal wavelets, entitled "Orthonormal wavelets". The key to multiresolution analysis is to design the scaling function of the wavelet such that it allowed other researchers to construct their own base wavelets in a mathematically grounded fashion. As an example, Daubechies (1988) created her own family of the wavelet, the Daubechies wavelets.

3.1.2 Wavelets for solution of PDEs

Wavelet is extensively used in signal and image processing but even though the theory of wavelet is already more than three decades old, a commercially viable PDEs solver in a wavelet basis is yet be to discovered. Nevertheless, in the literature, one can find many pioneering ideas utilizing the properties of wavelet for improving PDEs solvers from different angles. The motivations behind the use of wavelet bases for the numerical solution of partial differential equations may be best elucidated by means of the concept of multiresolution analysis. The idea is to interpolate an unknown (and irregular) field at a coarse level by means of so-called scaling functions. Any improvement to the initial approximation consists in adding 'details' (where needed) provided by new functions (wavelets) that are to be orthogonal or biorthogonal to the scaling functions.

The wavelet holds various desirable properties such as compact support, orthogonality, the exact representation of polynomials up to certain degree, as well as ability to represent functions at different resolutions. These advantages draw sight of mathematician and scholars to apply wavelets to the resolution of PDEs (Beylkin (1992), Qian and Weiss (1993 A), Amaratunga *et al.* (1994), Chen *et al.* (1996), Chen *et al.* (1996), Amaratunga and Williams (1997), Canuto *et al.* (2000), Cohen (2003)). The

compactly supported orthogonal Daubechies wavelets are used by Ko *et al.* (1995), Chen *et al.* (1996) and Youhe *et al.* (1998) for the Galerkin solution of PDEs. Fast wavelet transforms algorithm based on multiresolution analysis is demonstrated by Beylkin *et al.* (1991). It makes wavelet approximations attractive, and since then wavelet-based approximations have been utilized for the solution of ordinary and partial differential equations. Beylkin developed standard and nonstandard form of operators in wavelet bases. Harten (1995) demonstrated interpolating wavelets which are based on the interpolating subdivision scheme of (Deslauriers and Dubuc (1989)). This scheme has been employed to the numerical analysis by Vasilyev and Paolucci (1996).

The most common wavelet based projection techniques for numerical analysis are (i) the NS form of operators in the wavelet spaces (Beylkin *et al.* (1991), Beylkin and Keiser (1997)), (ii) wavelet Galerkin scheme (Amaratunga *et al.* (1992), Xu and Shann (1994), Pan (2003), Goedecker (2009), Mishra (2011)), (iii) wavelet-Taylor Galerkin approach (Mehra and Kumar (2005, 2007), Kumar and Mehra (2005)), and (iv) wavelet collocation schemes (Cai and Wang (1996), Vasilyev and Kevlahan (2005), Alam *et al.* (2006), Bertoluzza and Castro(2002)). The hurdle in the development of PDEs solver is due to difficulty in handling irregular boundary geometry and imposing boundary conditions. To impose proper boundary conditions in wavelet based methods several attempts are made such as (i) wavelets on an interval (Xu and Shann (1994), Latto *et al.* (1991)), (ii) proper extrapolation of data at the edge boundaries (Amaratunga and Williams (1997)), (iii) fictitious boundary conditions (Dianfeng *et al.* (1997), Kim *et al.* (2003), Jang *et al.* (2004)), and (iv) incorporation of boundary conditions with the capacitance matrix method (Williams and Amaratunga (1995)).

Lifting scheme has been developed by Swelden (1998) for the construction of

wavelets known as the second generation wavelets. The main feature of second generation wavelets is that the wavelets are constructed in the spatial domain and can be custom designed for complex domains and irregular sampling. Second generation wavelets supply the necessary freedom to deal with boundary conditions but with a cost of loss of translation invariance.

3.1.3 Wavelet based multiscale methods

Researchers have increased the usage of wavelets for the solution of PDEs after the development of the lifting scheme by Sweldens (1998) and stable completion (Carnicer *et al.* (1996), Dahmen (2001)). A review of wavelet techniques for the solution of PDEs has been presented by Dahmen (2001). The methods which use wavelets and scaling functions as basis functions and estimate inner products cannot compete with conventional FEM due to the cost of computing (Sandeep *et al.* (2011)).

Some researchers have combined the advantages of wavelet method with finite element, finite difference and finite volume methods to enhance the efficiency of wavelet based methods. Vasilyev and Paolucci (1996) have proposed a scheme that uses collocation method along with second generation wavelets to solve PDEs. D'Heedene *et al.* (2005) customized biorthogonal wavelets by using lifting scheme for the adaptive refinements of finite element space. Cohen *et al.* (2003) used wavelets with finite volume method (FVM) in the software QUADFLOW. Krysl *et al.* (2003) developed conforming hierarchical adaptive refinement methods. In general, second generation wavelets are preferred for coupling with finite element method (Quraishi and Sandeep (2011)).

In many cases, use of second generation wavelet is not essential, and the problems can be very efficiently solved by coupling well-known wavelets with very well developed

FEM. At present, we do not find any paper solving some of the very challenging problems by using simple coupling of wavelets with FEM. This will be particularly useful to those who are not very familiar with wavelets but are interested in applications where FEM/FDM/FVM requires a very fine mesh of uniform grid.

3.1.4 Wavelet based finite element method for wave propagation

Wave propagation can be characterized by the localized region of the sharp gradient of field variable which changes its locations in space with time. It is the area of vivid research. The conventional FEM (Langlet *et al.* (1995), Moser and Jacobs (1999), Semblat and Brioist (2000), Hassan and Veronesi (2003), Hosten and Castaings (2005), Greve *et al.* (2005), Mattsson and Nordström (2006), Moczo *et al.* (2007), Han *et al.* (2009)) which has been preferred for wave propagation, is not suitable to simulate higher harmonics. A drastic increase of nodes for such problems demands some necessary alteration in FEM, which must be numerically simple and efficient. Multiscale modeling is one possible solution for higher harmonics in wave propagation simulation. Recently, customized elements and geometric multiscale FEM have been developed to solve various types of wave propagation problems (Alleyne (1991), Kohno *et al.* (2010), Ham and Bathe (2012), Noh *et al.* (2013)). The wavelet based multiscale method leads to fast, hierarchical and locally adaptive algorithms. The potential of the wavelet is due to the compactly supported refinable basis functions (Meyer (1987), Liandrat and Tchamitchian (1990), Qian and Weiss (1993B), Strang and Nguyen (1996), Beylkin and Keiser (1997)).

As an example, we are presenting a case where cost of simulating higher harmonics of waves is very high. The requirement of very large number of nodes in FEM prohibits numerical simulation of higher harmonics of waves. Very large numbers of

nodes throughout the domain can be smartly avoided for this highly localized phenomenon. Wavelet coefficients are non-zero where burst signal exist and zero in the remaining part of the domain. Further, only some frequency components or wavelets are required to represent higher harmonics. These properties of wavelets are exploited in the current adaptive grid selection technique and multigrid solver. The nodes associated with detail coefficients, which are smaller than the preset tolerance, are ignored. In this process, the finest scale finite element solution space is projected as high- and low- frequency components onto wavelet spaces. A series of projections results in multi-scale decomposition of the fine scale solution into approximate solution and successive finer details. In the proposed wavelet projection method, FEM is preferred due to its capability to handle complex boundary and loading conditions instead of any other method. This multi-scale transformation hierarchically filters out the less significant frequencies and thus provides an effective framework to retain the necessary frequencies of the wave. In this process, the coefficient matrix at the finest level is calculated once for complete domain whereas the small adaptively compressed coefficient matrix is used in every marching step of the solution. Without involving any complex mathematical framework, the thesis presents a simple and general method to reduce the insignificant nodes in any wave propagation problems. Description of the necessary element of the algorithm in combination with mathematical comments on the method is provided to remove an implementation headache associated with adaptive grid techniques. The algorithm is applied to 2D plain strain problem, but it is general and independent of domain dimension.

3.2 Wavelet Overview

The several adaptations of scaled and transformation of the wavelet $\psi(\tau)$ construct

a family of wavelet functions. According to Daubechies (1988), the wavelet transform can be defined as, "*The wavelet transform is a tool that cuts up data, functions or operators into different frequency components, and then studies each component with a resolution matched to its scale.*" In the wavelet transformation, the basis functions span the space of square integrable functions $L^2(R)$ by translation and dilation of the compactly supported scaling function $\varphi(\tau)$ and detail function $\psi(\tau)$ (Daubechies (1988), Strang and Nguyen (1996), Walker (1999)).

3.2.1 Continuous wavelet transform (CWT)

The continuous wavelet transform is also called as the integral wavelet transform. Wavelet decomposition brings in the opinion of scale as an option to frequency and maps a signal into a time-scale domain, which is equivalent to the time-frequency domain used in the STFT. A wavelet is a function of zero average which is elaborated with a scale parameter and translated as:

$$\psi_{u,s}(t) = \frac{1}{\sqrt{s}}\psi\left(\frac{t-u}{s}\right) \tag{3.1}$$

Where the continuous variables s and u are scale and translation parameters, respectively. A wavelet family related with the mother wavelet $\psi(t)$ is produced by two parameters namely dilation and translation. The dilation or scale parameter, s, shows the width of the wavelet window. A lesser value of, s, implies the signal is studied by a narrower wavelet window in a lesser scale in other words higher resolution filtration. The translation or shift parameter, u suggests the position of the travelling wavelet window in the wavelet transform. Continuously changing wavelet window along the time axis implies analysing the signal in the current window position. Thus, information in the time

domain will remain unchanged. The continuous wavelet transform furnishes the decomposition of the signal $x(t)$ onto a set of basis functions that are worked out by an inner product of $x(t)$ with a mother wavelet $\psi(t)$, expressed as

$$Wx(u,s) = \frac{1}{\sqrt{s}} \int_{-\infty}^{\infty} x(t) * \psi^* \left(\frac{t-u}{s} \right) dt \; = < x(t), \psi_{u,s}(t) > \tag{3.2}$$

Where ψ^* denotes the complex conjugate of mother wavelet and symbol <,> denotes the inner product. The time domain signal is decomposed by time convolution with the scaled basis of function $\psi(t)$ called as simpler or daughter wavelets. The mother wavelet $\psi(t)$ can be complex Morlet wavelet, which provides the visualization of the possible discontinuities in signal.

The inverse CWT is defined as (Daubechies (1992)):

$$f(t) = \int_{-\infty}^{\infty} \int_{0}^{\infty} Wx(u,s) \psi_{u,s}(t) \, du \, ds \tag{3.3}$$

Translation parameter u is varying from 0 to ∞ and the range of scaling parameter s is from $-\infty$ to ∞. For most practical applications where the functions are evaluated at only a limited number of discrete points, there is no analytical solution for Eq. (3.2) and (3.3).

3.2.2 Discrete wavelet transform (DWT)

Discrete wavelet transform is employed to overcome the difficulties of the numerical implementation in using CWT for analytically unknown functions. Discrete wavelets can only be scaled and translated in discrete steps. Modification of equation (3.1) for the DWT can be expressed (Pahlavan (2012)) as:

$$\psi_{j,k}(t) = \frac{1}{\sqrt{s_0^j}} \psi\left(\frac{t - k u_0}{s_0^j} \right); \forall j, k \in \mathbb{Z} \tag{3.4}$$

The scaling factor $s_0 > 1$ suggests a fixed dilation step. It also affects the overall translation of the wavelet function. With an appropriate wavelet function and the specific choice of $s_0 = 2$ and $u_0 = 1$ providing dyadic sampling of the time and the frequency axes, the orthonormal basis $\left\{ \psi_{j,k} : j, k \in \mathbb{Z} \right\}$ can be generated such that

$$\left\langle \psi_{j,k}, \psi_{l,m} \right\rangle = \delta_{jl} \delta_{km} \tag{3.5}$$

in which δ_{jl} is the Kronecker delta and

$$\psi_{j,k}(t) = 2^{-j/2} \psi\left(2^{-j} t - k \right) \tag{3.6}$$

A function $f(t)$ can expressed in terms of the wavelet basis as:

$$f(t) = \sum_{j,k=-\infty}^{\infty} f_{j,k} \psi_{j,k}(t) \tag{3.7}$$

where $f_{j,k}$ are the transformation coefficients.

3.2.3 Multiscaling using wavelets

This section presents a promising numerical scheme for simulation of many harmonics in wave propagation. The wavelet based adaptive technique eliminates the requirement for a very large number of nodes in finite element method for propagation of such wave. This dynamic adaptive grid selection is based on the facts that very few wavelet coefficients are required to represent a short pulse containing higher harmonics.

The method is particularly useful where higher harmonics are ignored due to very high computational cost. The concept of multiscale analysis is to interpolate an unknown field at a coarse level with the help of so-called scaling functions. Any improvement to the initial approximation is achieved by adding ‘details' provided by new functions known as wavelets. A multiscaling analysis forms a sequence of closed subspaces to satisfy certain self-similarity relations as well as completeness and regularity relations.

(A) Self-similarity in time and scale: it requires each subspace V_k as dyadic invariant under shifts by integer multiples of 2^k and all subspaces are time-scaled versions of each other with a dilation factor 2^{k-l}, i.e. for each $f \in V_k$

$$f(x) \in V_j \Leftrightarrow f(2x) \in V_{j+1} \tag{3.8a}$$

$$f(x) \in V_0 \Leftrightarrow f(x+1) \in V_0 \tag{3.8b}$$

(B) The sequencing of subspaces should follow, for $k > j$ the space resolution 2^j of the j^{th} subspace is lower than the resolution 2^k of the k^{th} subspace.

$$V_0 \subset V_1 \subset V_2 \subset ..V_j .. \subset V_k ... L^2(R) \tag{3.9}$$

(C) Regularity: It is required that the model subspace V_0 should be generated as the linear combination of a finite number of generating functions $\phi_1 ..... \phi_r$, and their integer shifts, at least, form a frame for the subspace $V_0 \subset L^2(R)$. These functions are also known as scaling functions. In most cases the basic requirement for these functions is to be piecewise continuous with compact support.

(D) Completeness: It is required that the nested subspaces fill the whole space, i.e. their union should be dense in $L^2(R)$, and intersection should contain the zero elements i.e.

$\overline{\cup V_j}$ is dense in $L^2(R)$; $\cap V_j = \{0\}$.

Each subspace V_j is spanned by a set of scaling function $\{\phi_{j,k}(x), \forall k \in Z\}$. The complement of V_j in V_{j+1} is defined as subspace W_j such that

$$V_{j+1} = V_j \oplus W_j \qquad \forall j \in Z \tag{3.10a}$$

The space V_{j+1} can be decomposed in a consecutive manner as:

$$V_{j+1} = V_0 \oplus W_0 \oplus W_1 \oplus W_2 ... \oplus W_j \tag{3.10b}$$

The basis functions in W_j are called wavelet functions and are denoted by $\psi_{j,k}$. These wavelets and scaling functions are used for wavelet based multiscaling. Scaling and wavelet functions are shown in Figures (3.1) -(3.3) for Haar, Daubechies, and B-spline wavelet respectively. A function $f \in L^2(R)$ is approximated by its projection $P^j f$ onto the space V_j and the projection of f on W_j as $Q^j f$, we have

$$P^j f = P^{j-1} f + Q^{j-1} f \tag{3.11}$$

If the coefficient vector of $P^j f$ in terms of some scaling function basis is $\mathbf{C}_j = \{C_{j,0}, ..., C_{j,v(j)}\}^T$ and coefficient vector of $Q^j f$ in terms of some wavelet basis is $\mathbf{d}_j = \{d_{j,0}, ..., d_{j,w(j)}\}^T$ then we can write wavelet transform as

$$\mathbf{C}_j = [\mathbf{P}_j \,|\, \mathbf{Q}_j] \begin{bmatrix} \mathbf{C}_{j-1} \\ \mathbf{d}_{j-1} \end{bmatrix} \tag{3.12}$$

where $2^j \times 2^{j-1}$ is the size of $\mathbf{P}_j$ and $\mathbf{Q}_j$ matrices. In this thesis, Haar wavelet, B-spline wavelet (Stollnitz *et al.* (1996)), and Daubechies (D4) wavelet are used for numerical simulation.

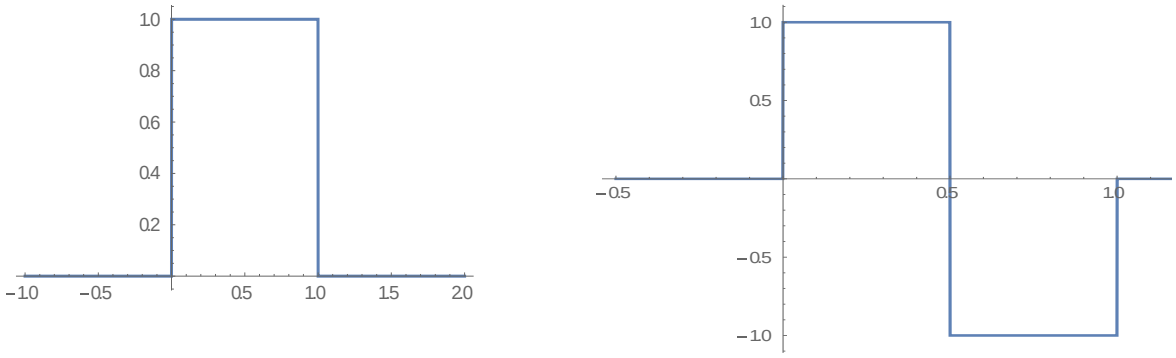

(a) scaling (b) wavelet

Figure 3.1. Haar scaling and wavelet function

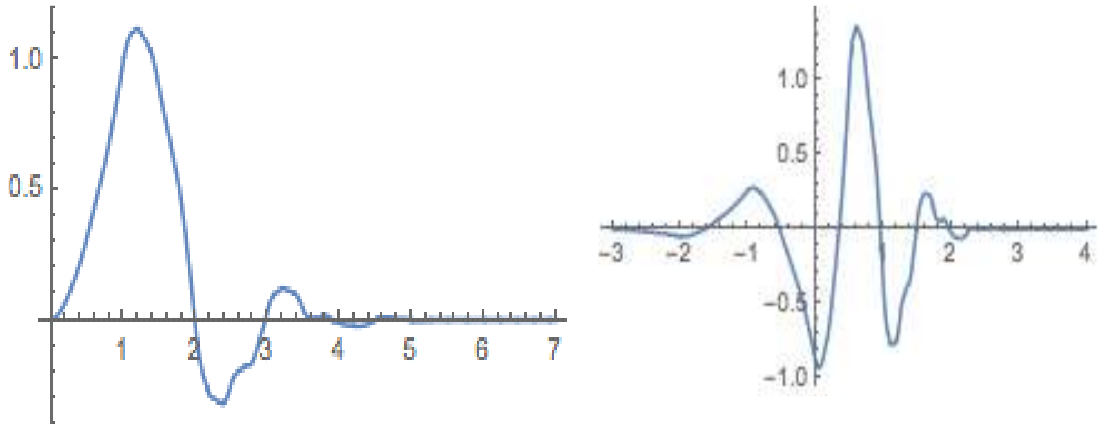

(a) scaling (b) wavelet

Figure 3.2. D_4 scaling and D_4 wavelet function

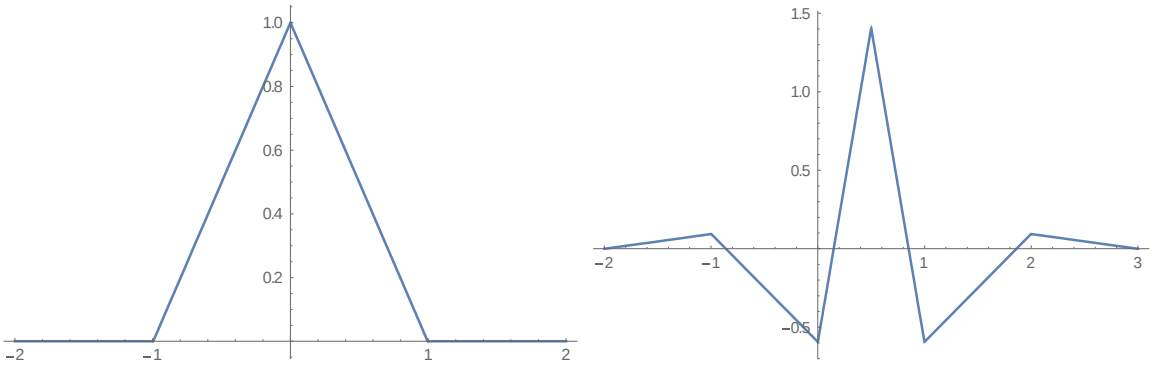

(a) scaling (b) wavelet

Figure 3.3. B-spline scaling and B-spline wavelet function

The synthesis matrices $\mathbf{P}_j$ and $\mathbf{Q}_j$ for Haar wavelet are:

$$\mathbf{P}_j = \begin{bmatrix} \alpha_1 & \alpha_2 & 0 & 0 & 0 & 0 & . & . & . & . & . & . & . & . & . & . & 0 & 0 \\ 0 & 0 & \alpha_1 & \alpha_2 & 0 & 0 & 0 & 0 & . & . & . & . & . & . & . & . & 0 & 0 \\ . & . & . & . & . & . & . & . & & & & & . & & & & . & . \\ . & . & . & . & . & . & . & . & & & & & . & & & & . & . \\ . & . & . & . & . & . & . & . & & & & & . & & & & . & . \\ 0 & 0 & 0 & 0 & 0 & 0 & . & . & . & . & . & . & . & . & . & . & \alpha_1 & \alpha_2 \end{bmatrix} \quad (3.13a)$$

$$\mathbf{Q}_j = \begin{bmatrix} \beta_1 & \beta_2 & 0 & 0 & 0 & 0 & . & . & . & . & . & . & . & . & . & . & 0 & 0 \\ 0 & 0 & \beta_1 & \beta_2 & 0 & 0 & 0 & 0 & . & . & . & . & . & . & . & . & 0 & 0 \\ . & . & . & . & . & . & . & . & & & & & . & & & & . & . \\ . & . & . & . & . & . & . & . & & & & & . & & & & . & . \\ . & . & . & . & . & . & . & . & & & & & . & & & & . & . \\ 0 & 0 & 0 & 0 & 0 & 0 & . & . & . & . & . & . & . & . & . & . & \beta_1 & \beta_2 \end{bmatrix} \quad (3.13b)$$

The constants α_i and β_i are defined as:

$$\left.\begin{array}{ll} \alpha_1 = \dfrac{\sqrt{2}}{2}, & \alpha_2 = \dfrac{\sqrt{2}}{2} \\ \beta_1 = \dfrac{\sqrt{2}}{2}, & \beta_1 = -\dfrac{\sqrt{2}}{2} \end{array}\right\} \quad (3.13c)$$

The synthesis matrices $\mathbf{P}_j$ and $\mathbf{Q}_j$ for Daubechies (D4) wavelet are:

$$\mathbf{P}_j = \begin{bmatrix} \alpha_1 & \alpha_2 & \alpha_3 & \alpha_4 & 0 & 0 & . & . & . & . & . & . & . & . & . & 0 & 0 \\ 0 & 0 & \alpha_1 & \alpha_2 & \alpha_3 & \alpha_4 & 0 & 0 & . & . & . & . & . & . & . & 0 & 0 \\ . & . & . & . & . & . & . & . & & & & . & & & & . & . \\ . & . & . & . & . & . & . & . & & & & . & & & & . & . \\ . & . & . & . & . & . & . & . & & & & . & & & & . & . \\ \alpha_3 & \alpha_4 & 0 & 0 & 0 & 0 & . & . & . & . & . & . & . & . & . & \alpha_1 & \alpha_2 \end{bmatrix} \quad (3.14a)$$

$$\mathbf{Q}_j = \begin{bmatrix} \beta_1 & \beta_2 & \beta_3 & \beta_4 & 0 & 0 & . & . & . & . & . & . & . & . & . & 0 & 0 \\ 0 & 0 & \beta_1 & \beta_2 & \beta_3 & \beta_4 & 0 & 0 & . & . & . & . & . & . & . & 0 & 0 \\ . & . & . & . & . & . & . & . & & & & . & & & & . & . \\ . & . & . & . & . & . & . & . & & & & . & & & & . & . \\ . & . & . & . & . & . & . & . & & & & . & & & & . & . \\ \beta_3 & \beta_4 & 0 & 0 & 0 & 0 & . & . & . & . & . & . & . & . & . & \beta_1 & \beta_2 \end{bmatrix} \quad (3.14b)$$

The constants α_i and β_i are defined as:

$$\left.\begin{aligned} \alpha_1 = \frac{1+\sqrt{3}}{4\sqrt{2}}, \quad \alpha_2 = \frac{3+\sqrt{3}}{4\sqrt{2}}, \quad \alpha_3 = \frac{3-\sqrt{3}}{4\sqrt{2}}, \quad \alpha_4 = \frac{1-\sqrt{3}}{4\sqrt{2}} \\ \beta_1 = \frac{1-\sqrt{3}}{4\sqrt{2}}, \quad \beta_1 = \frac{\sqrt{3}-3}{4\sqrt{2}}, \quad \beta_3 = \frac{3+\sqrt{3}}{4\sqrt{2}}, \quad \beta_4 = \frac{-1-\sqrt{3}}{4\sqrt{2}} \end{aligned}\right\} \quad (3.14c)$$

The synthesis matrices $\mathbf{P}_j$ and $\mathbf{Q}_j$ for B-spline wavelet are:

$$\mathbf{P}_j = \frac{1}{2}\begin{bmatrix} 2 & 0 & . & . & . & . & . & 0 \\ 1 & 1 & 0 & . & . & . & . & 0 \\ 0 & 2 & 0 & . & . & . & . & . \\ . & 1 & 1 & . & . & . & . & . \\ . & 0 & 2 & . & . & . & . & . \\ . & . & 1 & . & . & . & . & . \\ . & . & 0 & . & . & . & . & . \\ . & . & . & . & . & . & 1 & . \\ . & . & . & . & . & . & 2 & . \\ 0 & 0 & . & . & . & . & 1 & 1 \\ 0 & 0 & . & . & . & . & 0 & 2 \end{bmatrix} \quad (3.15a)$$

$$\mathbf{Q}_j = \sqrt{\frac{2^j}{72}} \begin{bmatrix} -11.022704 & 0 & . & . & . & . & . & 0 \\ 10.104145 & 1 & 0 & . & . & . & . & . \\ -5.511352 & -6 & 0 & . & . & . & . & . \\ 0.918559 & 10 & 1 & 0 & . & . & . & . \\ 0 & -6 & -6 & 0 & . & . & . & . \\ . & 1 & 10 & . & . & . & . & . \\ . & 0 & -6 & . & . & . & . & . \\ . & . & 1 & . & . & . & 1 & . \\ . & . & 0 & . & . & . & -6 & . \\ . & . & . & . & . & . & 10 & 0.918559 \\ . & . & . & . & . & . & -6 & -5.511352 \\ . & . & . & . & . & . & 1 & 10.104145 \\ 0 & . & . & . & . & . & 0 & -11.022704 \end{bmatrix} \tag{3.15b}$$

3.2.4 Multi-scale decomposition of finite element matrix using wavelets

Consider a dynamic equation discretized into the set of finite element equations as:

$$[K][u]+[M][\ddot{u}]=0 \tag{3.16}$$

Where $[K]$ is global stiffness matrix and $[M]$ is a global mass matrix, $[u]$ and $[\ddot{u}]$ are unknown coefficient vectors. The marching variable $[\mathrm{u}]_{s+1}$ of the dynamic equation at time t_{s+1} can be obtained from the coefficients $[\mathrm{u}]_s$ at t_s by using the recursive relation of α - family of approximation (Reddy (2005)).

$$\{[M]+\Delta t\alpha[K]\}[\mathrm{u}]_{s+1}=\{[M]-(1-\alpha)\Delta t[K]\}[\mathrm{u}]_s \tag{3.17}$$

$$[\hat{K}][\mathrm{u}]_{s+1}=[\tilde{K}][\mathrm{u}]_s \tag{3.18}$$

This equation at the finest resolution j and can be expressed as:

$$\left[K_j^u\right]\left[u_j\right]=\left[f_j\right] \tag{3.19}$$

Using wavelets for forward transformation $T_j=\left[P_j \mid Q_j\right]$, the finest scale is replaced by multiscale, which can be expressed as

$$\left[T_j\right]\begin{bmatrix} d_{j-1} \\ u_{j-1} \end{bmatrix}=\left[u_j\right] \tag{3.20}$$

substituting Eq. (3.20) in Eq. (3.19), we get

$$\left[K_j^u\right]\left[T_j\right]\begin{bmatrix} d_{j-1} \\ u_{j-1} \end{bmatrix}=\left[f_j\right] \tag{3.21}$$

or

$$\left[T_j^T\right]\left[K_j^u\right]\left[T_j\right]\begin{bmatrix} d_{j-1} \\ u_{j-1} \end{bmatrix}=\left[T_j^T\right]\left[f_j\right] \tag{3.22}$$

where u_{j-1} are the scaling coefficients, d_{j-1} are the wavelets coefficient at the lower resolution. After wavelet transform, the set of equations can be expressed as:

$$\begin{bmatrix} \left[k_{d_{j-1}}^{d_{j-1}}\right] & \left[k_{u_{j-1}}^{d_{j-1}}\right] \\ \left[k_{d_{j-1}}^{u_{j-1}}\right] & \left[k_{u_{j-1}}^{u_{j-1}}\right] \end{bmatrix}\begin{bmatrix} \left[d_{j-1}\right] \\ \left[u_{j-1}\right] \end{bmatrix}=\begin{bmatrix} \left[f_{j-1}^d\right] \\ \left[f_{j-1}^u\right] \end{bmatrix} \tag{3.23}$$

The solution can be transformed back in terms of nodal displacement by inverse wavelet transform using Eq. (3.20). Similarly, refinement at the next level can be expressed as:

$$\left[T_{j-1}^T\right]\begin{bmatrix} \left[k_{d_{j-1}}^{d_{j-1}}\right] & \left[k_{u_{j-1}}^{d_{j-1}}\right] \\ \left[k_{d_{j-1}}^{u_{j-1}}\right] & \left[k_{u_{j-1}}^{u_{j-1}}\right] \end{bmatrix}\left[T_{j-1}\right]\begin{bmatrix} d_{j-2} \\ d_{j-1} \\ u_{j-2} \end{bmatrix}=\left[T_{j-1}^T\right]\begin{bmatrix} f_{j-1}^d \\ f_{j-1}^u \end{bmatrix} \tag{3.24}$$

These equations are expressed in the standard form after application of next level of wavelet transformation as:

$$\begin{bmatrix} \left[k_{d_{j-1}}^{d_{j-1}}\right] & \left[\left[k_{d_{j-2}}^{d_{j-1}}\right] & \left[k_{u_{j-2}}^{d_{j-1}}\right]\right] \\ \left[\left[k_{d_{j-1}}^{d_{j-2}}\right]\right] & \left[\left[k_{d_{j-2}}^{d_{j-2}}\right] & \left[k_{u_{j-2}}^{d_{j-2}}\right]\right] \\ \left[\left[k_{d_{j-1}}^{u_{j-2}}\right]\right] & \left[\left[k_{d_{j-2}}^{u_{j-2}}\right] & \left[k_{u_{j-2}}^{u_{j-2}}\right]\right] \end{bmatrix} \begin{bmatrix} \left[d_{j-1}\right] \\ \left[d_{j-2}\right] \\ \left[u_{j-2}\right] \end{bmatrix} = \begin{bmatrix} \left[f_{j-1}^{d}\right] \\ \left[f_{j-2}^{d}\right] \\ \left[f_{j-2}^{u}\right] \end{bmatrix} \tag{3.25}$$

The wavelet transform can be continued until a desired low and high-frequency component representation is achieved.

Our overall process for single pass filtering i.e. application on x direction can be expressed as:

$$u_j(x) \rightarrow u_{j-1}(x) \rightarrow u_{j-2}(x) \rightarrow \ldots \rightarrow u_0(x)$$

$$\searrow \qquad \searrow \qquad \qquad \searrow$$

$$d_{j-1}(x) \quad d_{j-2}(x) \quad \ldots \quad d_0(x)$$

Multiplication of stiffness matrix with the all level of transformation matrices will lead to a new structure of coefficient matrix which is shown as 16 blocks.

$V_0 \times V_0$	$V_0 \times W_0$	$V_0 \times W_1$	$V_0 \times W_2$
$W_0 \times V_0$	$W_0 \times W_0$	$W_0 \times W_1$	$W_0 \times W_2$
$W_1 \times V_0$	$W_1 \times W_0$	$W_1 \times W_1$	$W_1 \times W_2$
$W_2 \times V_0$	$W_2 \times W_0$	$W_2 \times W_1$	$W_2 \times W_2$

Retaining grid points associated with wavelets coefficients at high gradient region and eliminating them from *a priori* known smooth region will generate the adaptive grid. The objective of multi-scale is to represent higher harmonics with less number of detail coefficients and develop a compressed stiffness matrix from the finest scales solution.

Meshing the whole domain with very fine mesh to simulate higher harmonics is unaffordable but the method becomes considerably less expensive to solve after elimination of insignificant detail coefficients. There is no need of re-meshing the FE domain and re-computing the stiffness matrix with the change in location of the wave.

The finite element solution depends on the mesh resolution and is calculated at the associated grid points /nodes of the mesh. Here we denote $T_j \in \mathrm{N}$ as the set of indices representing the nodes of space V_j. $M_{j-1} \in \mathrm{N}$ represents the nodes belonging to the added details. In Figure 3.4 (a) the refined space V_j has nodes $(1..91) \in T_j$, Figure 3.4 (b) shows the decomposition of space $V_{j-1} \oplus W_{j-1}$. Here $(n1..n63) \in M_{j-1}$, and $(m1..m28) \in T_{j-1}$

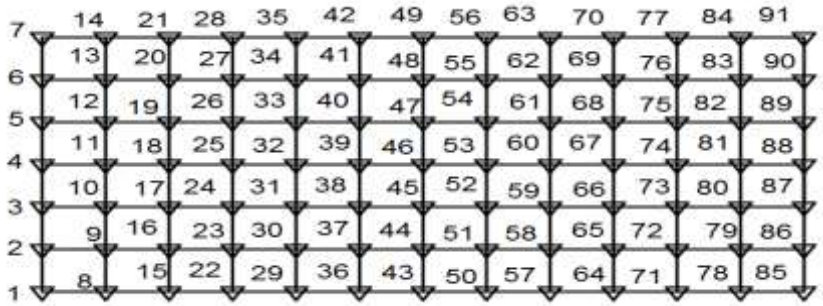

(a) Space V_j

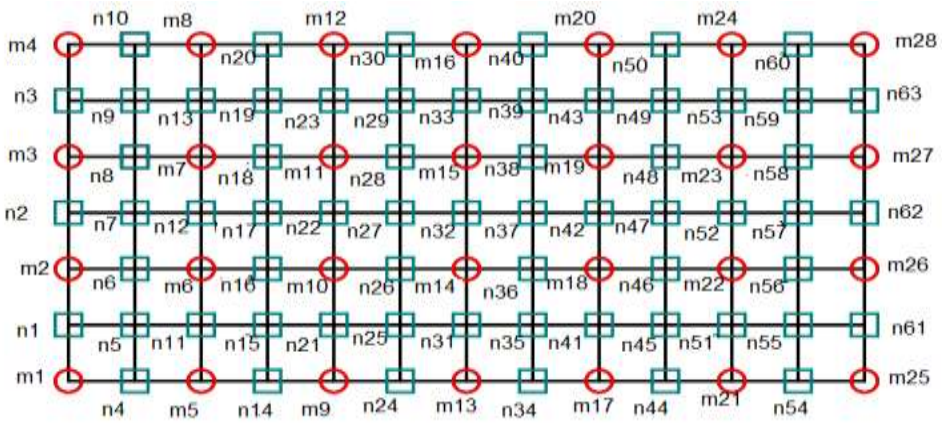

(b) Space $V_{j-1} \oplus W_{j-1}$

Figure 3.4. Multi-scale decomposition

The basic idea behind the adaptive solution is simply based on the analysis of wavelet coefficients, which gives information about the region where sharp change is starting or ending. This wavelet based multiscale transformation hierarchically filters out the insignificant part of the solution and thus provides an effective framework for the selection of significant part of the solution. The location of fine grid changes with the change in the position of the sharp gradient. To reduce error due to end effects, the computational grid should include points near the sharp gradient zone also. In this process, we include those grid points whose wavelets coefficients will become significant during the next moving step of the wave. Constant strain triangles with uniformly distributed nodes throughout the plate and four elements along the thickness are used. In this process, the 'big' coefficient matrix at the finest level is calculated once for complete domain. In all subsequent steps the 'small' adaptively compressed coefficient matrix for the dynamic zone of high gradient, which is considerably less expensive to solve, is used for the solution. Finite element stiffness matrix at the finest scale is transformed to the wavelet space only once. The size of stiffness matrix is reduced by eliminating rows and column associated with the smooth region in all subsequent steps of the adaptive solution. The method is not only suitable to develop the compressed stiffness matrix and to eliminate the process of re-meshing the FE domain but also to propagate higher harmonics of waves using least number of nodes.

3.3 Numerical Results

The fundamentals of wavelet analysis and the necessary mathematical background, as well as wavelet applications, are elaborately discussed in the previous sections. In this section, a multiscale approach is used in order to solve linear and

nonlinear wave propagation problems in plate-like structure. The potential of the proposed method is analyzed using several examples, and results are compared with the conventional finite element method.

In this section, we illustrate the performance of the wavelet based multi-scale method by solving several wave propagation problems. First, we solve transient scalar and time harmonic wave equations. Then, we use the method to solve for the Lamb wave in the square plate structure and focus on the sharpness of the wave front. At the end, guided Lamb wave propagation problem is solved which contains higher harmonics.

3.3.1 Transient scalar wave

In this numerical experiment, we consider a transient scalar wave equation with Ricker wavelet source at the center of a two-dimensional domain, (Han and Bathe (2012), Yue and Guddati (2005)):

$$\frac{\partial^2 u}{\partial x^2}+\frac{\partial^2 u}{\partial y^2}+F\left(0,0,t\right)=\frac{1}{C^2}\frac{\partial^2 u}{\partial t^2} \tag{3.26}$$

$$F\left(0,0,t\right)=10\left(1-2\pi^2 f^2\left(t-0.25\right)^2\exp\left(-\pi^2 f^2\left(t-0.25\right)^2\right)\right) \tag{3.27}$$

Where C is the wave velocity, u is the displacement solution, f is the central frequency. In this case $C=1$ and $f=6\,\text{Hz}$ is considered. Due to symmetry, only the upper right quadrant of the domain $\left[0,1\right]\times\left[0,1\right]$ is considered for the solution. We let the wave propagate only for 0.95 s, i.e. before it hits the boundaries so no absorbing boundary is necessary. We choose a very small time-step $\Delta t=0.00625\,\text{s}$.

To validate the present wavelet based solution methodology for wave propagation problems, the displacement response of the transient scalar wave is obtained for different element size and depicted in Figure 3.5. We observe some spurious wave in 60×60 and 80×80 mesh which disappeared in 100×100 mesh. Snapshots of displacements at different time instants with 100×100 mesh number are shown in Figure 3.6. Boundary reflection can be observed in the same figure if simulation time is greater than t = 0.95 s. To capture wave in the plates, FEM uses 100×100 uniformly distributed nodes while half of the FEM nodes are required after application of one level of wavelet transform. Displacement variations along the x-axis at t = 0.95 s obtain from present method is compared with the results due to Han and Bathe (2012) based on finite element method in Figure 3.7. It is observed that the results are in good agreement. It shows that proposed multiscale method provides computationally efficient adaptive solution with a better approximation capability when solving singularity or high gradient problems in engineering. The multiresolution representation of the field solution can be used to reduce the number of unknowns. For areas with a smooth field distribution, wavelet coefficients that describe finer details become very small and can therefore be neglected. This is equivalent to a local reduction of the discretization density.

3.3.2 Time harmonic scalar wave

In the second numerical experiment, we consider a time harmonic scalar wave equation (Han and Bathe (2012)):

$$\frac{\partial^2 u}{\partial x^2}+\frac{\partial^2 u}{\partial y^2}+k^2u=0, \qquad 0\le x\le 2 \ and \ 0\le y\le 2 \tag{3.28}$$

where u is displacement, and $k=8\pi \ in \ 0\le x\le 1 \ and \ k=4\pi \ in \ 1\le y\le 2$. The boundary

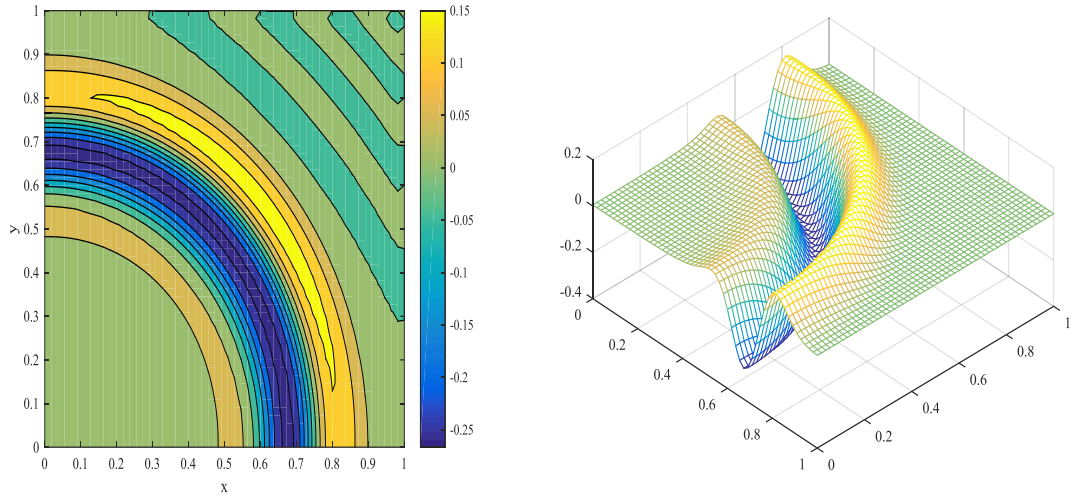

(a) 60×60 mesh

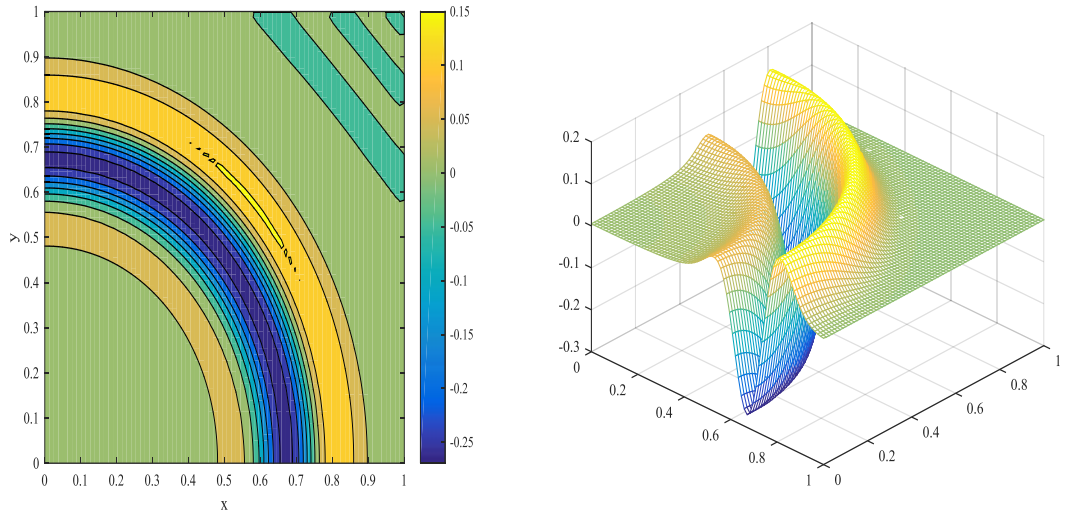

(b) 80×80 mesh

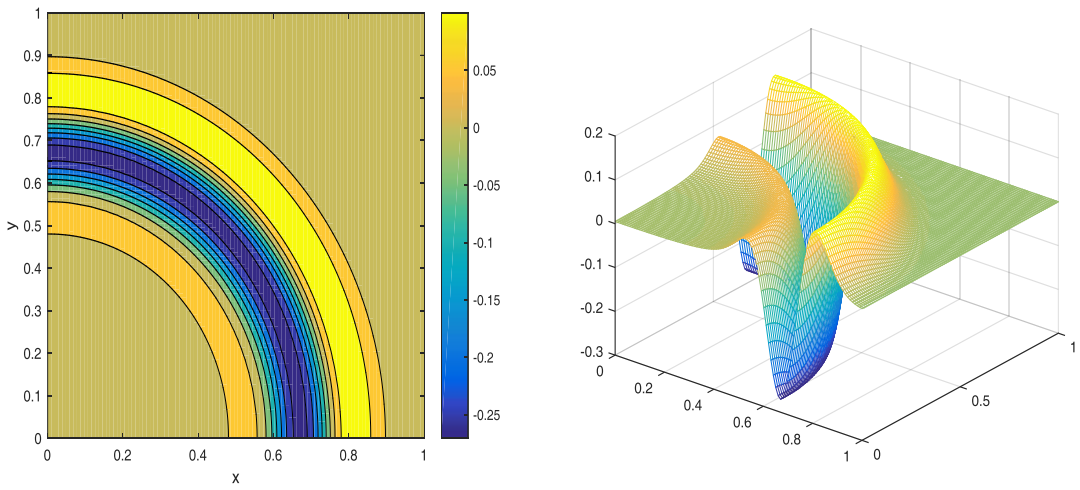

(c) 100×100 mesh

Figure 3.5. Snapshots of displacements at t = 0.95 s with various mesh number

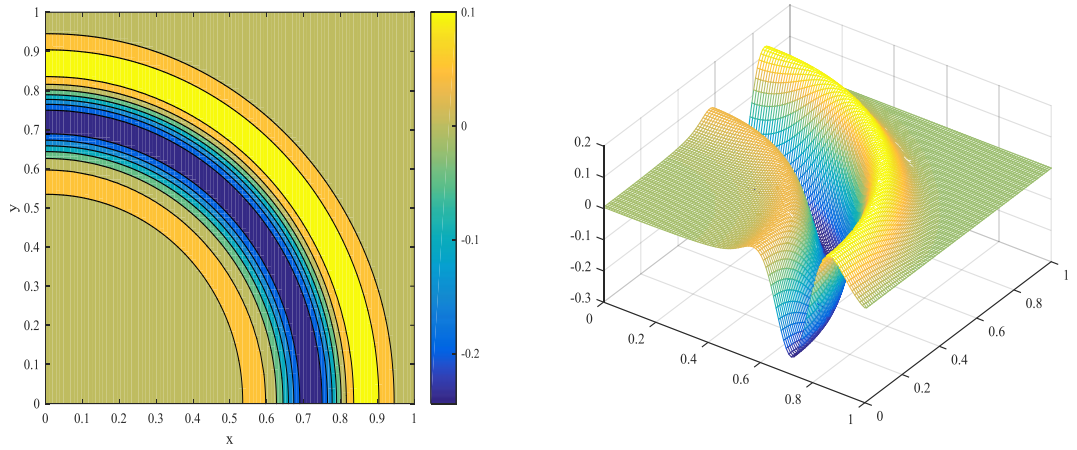

(a) Displacements at t = 0.62 s

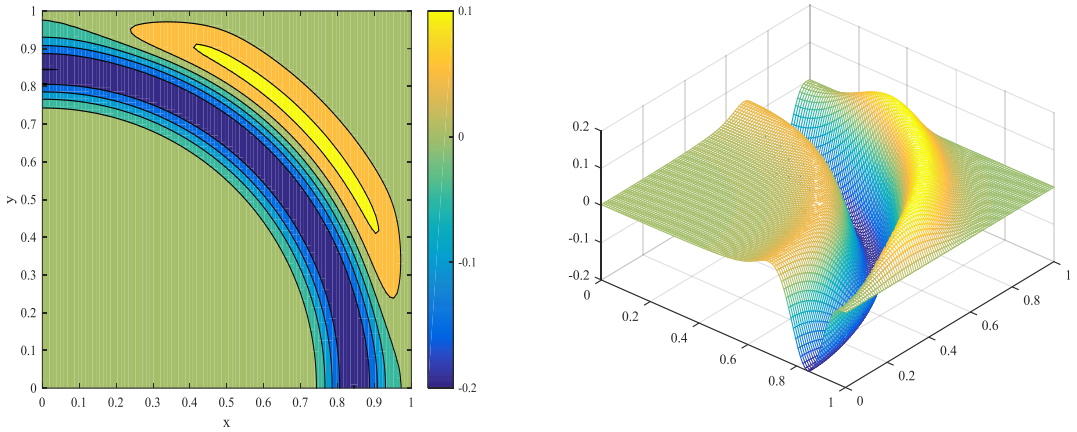

(b) Displacements at t = 1.062 s

Figure 3.6. Snapshots of displacements at different time instants with 100×100 mesh number

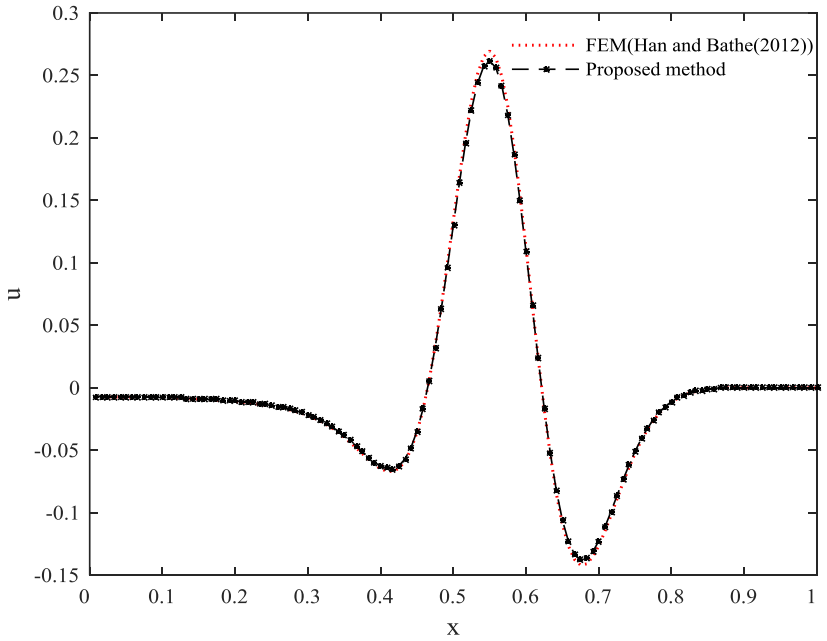

Figure 3.7. Displacement variations along the x-axis at t = 0.95 s

conditions are:

$$u(0,\mathrm{y})=0,\quad \frac{\partial u(x,2)}{\partial y}=0,\quad \frac{\partial u(x,0)}{\partial y}=0,\ \text{and}\ \frac{\partial u(2,y)}{\partial x}=4\pi \tag{3.29}$$

This is one-dimensional problem but it is a useful problem to examine the error occurring in numerical techniques. To assess the accuracy of the solution, displacement variations along the x-axis obtain from present method is compared with the results from finite element method with 100×100 mesh in Figure 3.8. Similar to previous problem, FEM uses 100×100 uniformly distributed nodes while half of the FEM nodes are required after application of one level of wavelet transform. The numerical result confirms the multiresolution properties of the wavelet based method, which reveals that the technique is useful. The proposed method reduces the computation time and number of degrees of freedom needed to solve wave propagation problems.

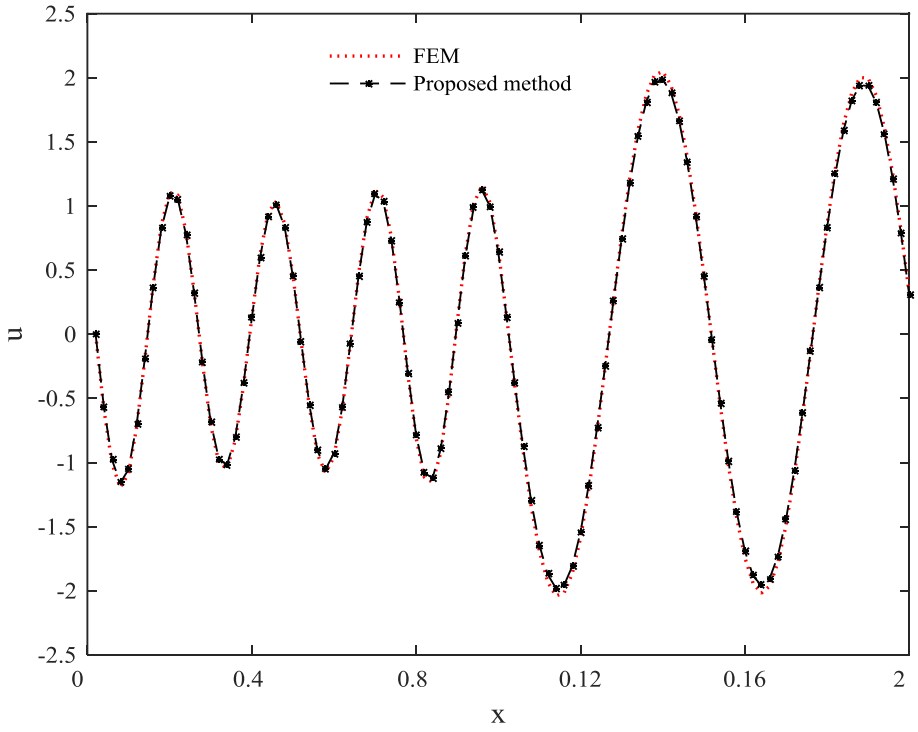

Figure 3.8. Displacement variations along the x-axis.

The numerical solution of displacement response u for time harmonic scalar wave is presented with 100×100 mesh in Figure 3.9. This figure ensures the reliability of the proposed method.

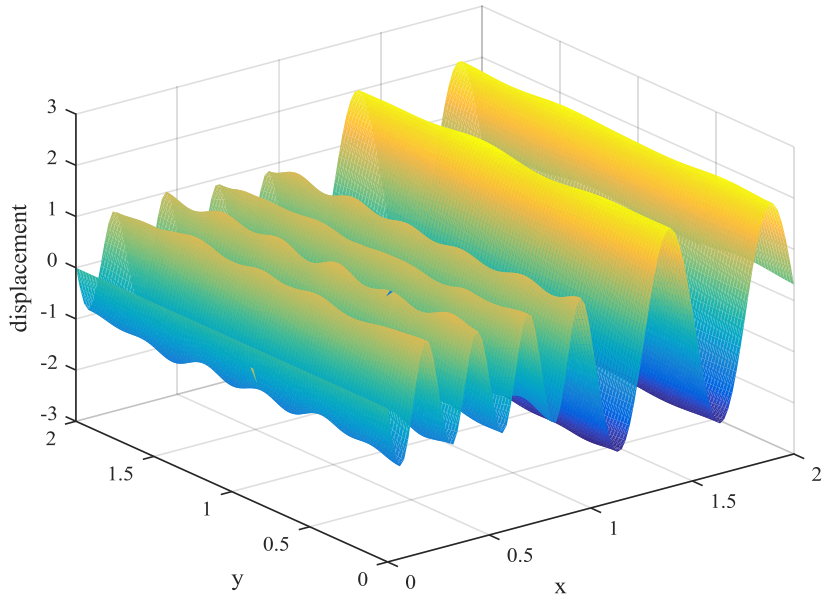

(a) FEM solutions with 100×100 mesh for time harmonic scalar wave

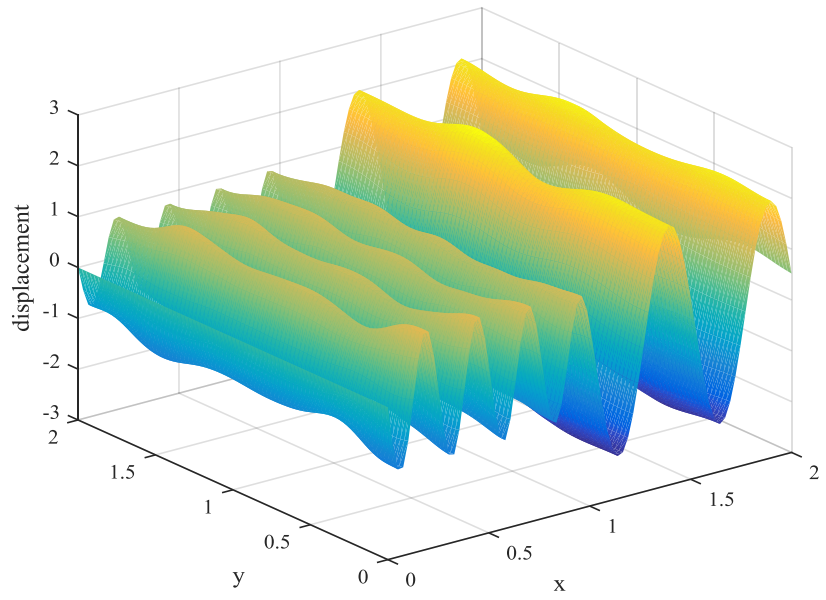

(b) Wavelet based solutions for time harmonic scalar wave

Figure 3.9. Displacement response u for time harmonic scalar wave

3.3.3 Lamb waves

In order to evaluate the performance of proposed multiscale method for two dimensional and two variables problem, we consider Lamb waves. Lamb wave can be expressed using longitudinal velocity C_L and shear velocity C_T as:

$$C_L^2 \frac{\partial^2 u}{\partial x^2} + (C_L^2 - C_T^2) \frac{\partial^2 v}{\partial x \partial y} + C_T^2 \frac{\partial^2 u}{\partial y^2} = \frac{\partial^2 u}{\partial t^2} \tag{3.30a}$$

$$C_L^2 \frac{\partial^2 v}{\partial y^2} + (C_L^2 - C_T^2) \frac{\partial^2 u}{\partial x \partial y} + C_T^2 \frac{\partial^2 v}{\partial x^2} = \frac{\partial^2 v}{\partial t^2} \tag{3.30b}$$

Where $C_L^2 = \lambda + 2\mu/\rho$ and $C_T^2 = \mu/\rho$. $\lambda = Ev/(1+v)(1-2v)$ and $\mu = E/2(1+v)$ are Lamé constants. E and v are Young's modulus and Poisson ratio, respectively.

In this example, a 50 x 50 mm^2 homogeneous isotropic Al plate (density=2700 kg/m^3) is considered. 2500 uniformly distributed FE elements and one level of wavelet transform are used to capture wave in the plates. The simulation of Lamb wave using wavelet-based multiscale method in the plate with 400 kHz central frequency is presented in Figure 3.10. Contour plots of the displacement in the x-direction at four different time instants is well depicted in the Figure. Figure 3.11(a) depicts the five cycle modulated sinusoidal Hanning-window excitation signal of linear Lamb wave at 400 kHz. These Lamb waves have been used for detection of cracks in the plates (Greve et al.). The higher harmonics in these investigations were ignored due to high computational cost. To see the efficiency of the wavelet-based method, higher harmonics are added in the Lamb wave and propagation of waves are observed. This study uses the following actuation function with 400 kHz central frequency driven through a Hanning window:

$$F(t)=\begin{cases} A_o \sin(\omega t)*\left(\sin(\frac{\omega t}{10})\right)^2+\frac{A_o}{10}\sin(10\omega t)*\left(\sin(\omega t)\right)^2, & t<\frac{10\pi}{\omega} \\ 0, & \textit{otherwise.} \end{cases} \quad (3.39)$$

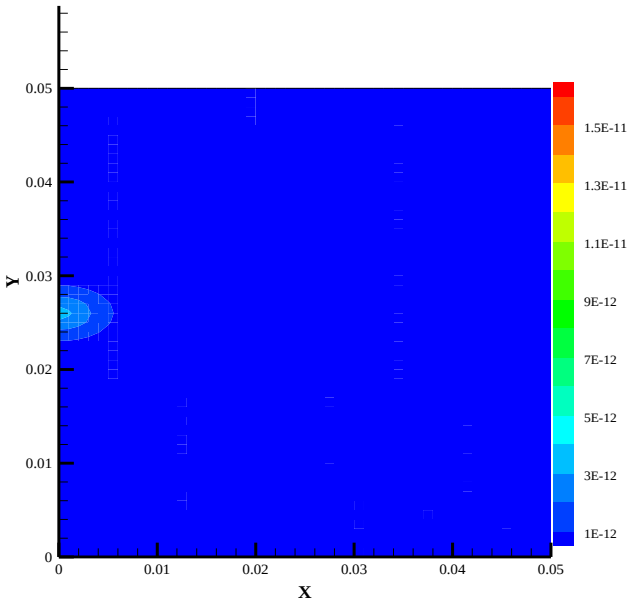

(a) 5 μs

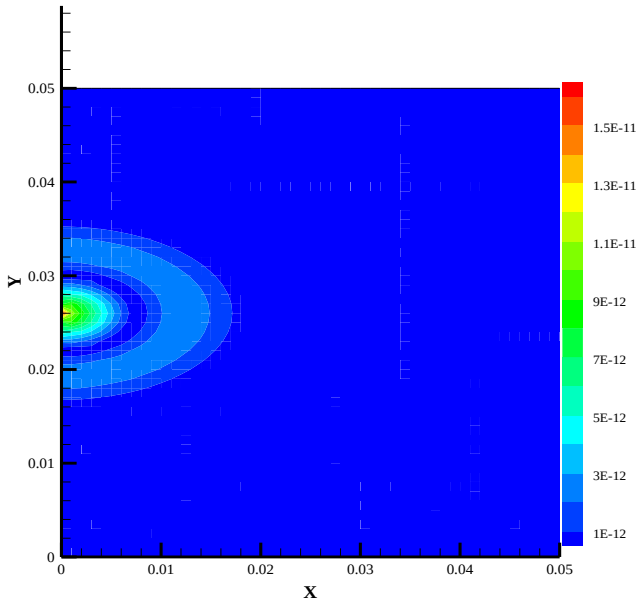

(b) 20 μs

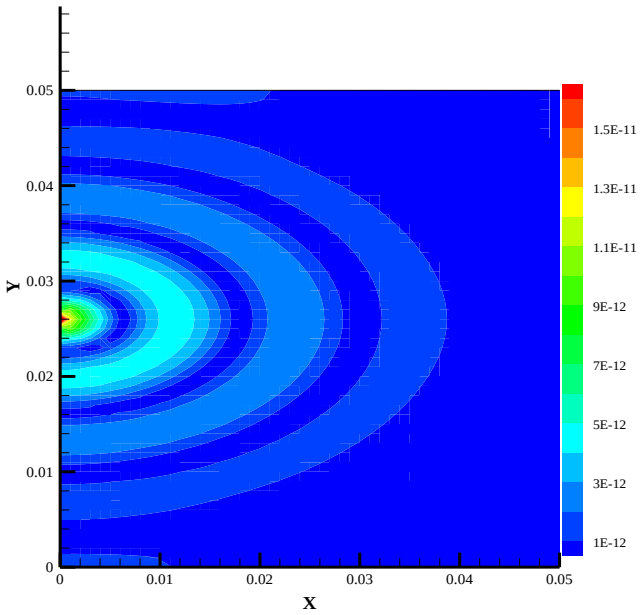

(c) 35 μs

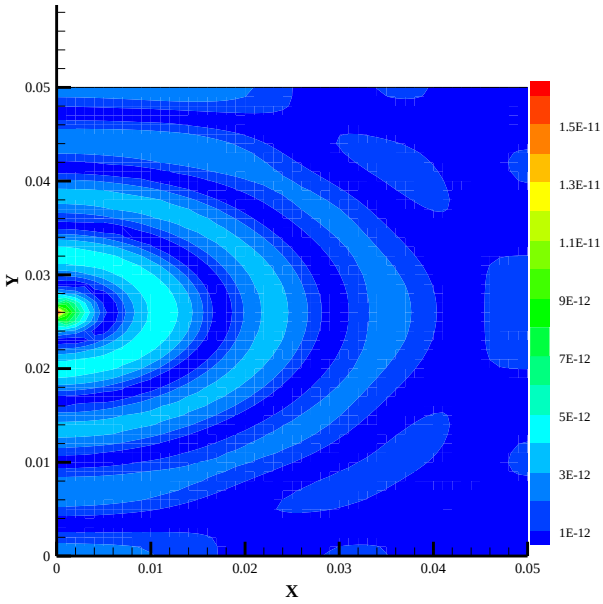

(d) 50 μs

Figure 3.10. Contour plots of the displacement in the x-direction at three different time frame for isotropic plate by wavelet-based multiscale method

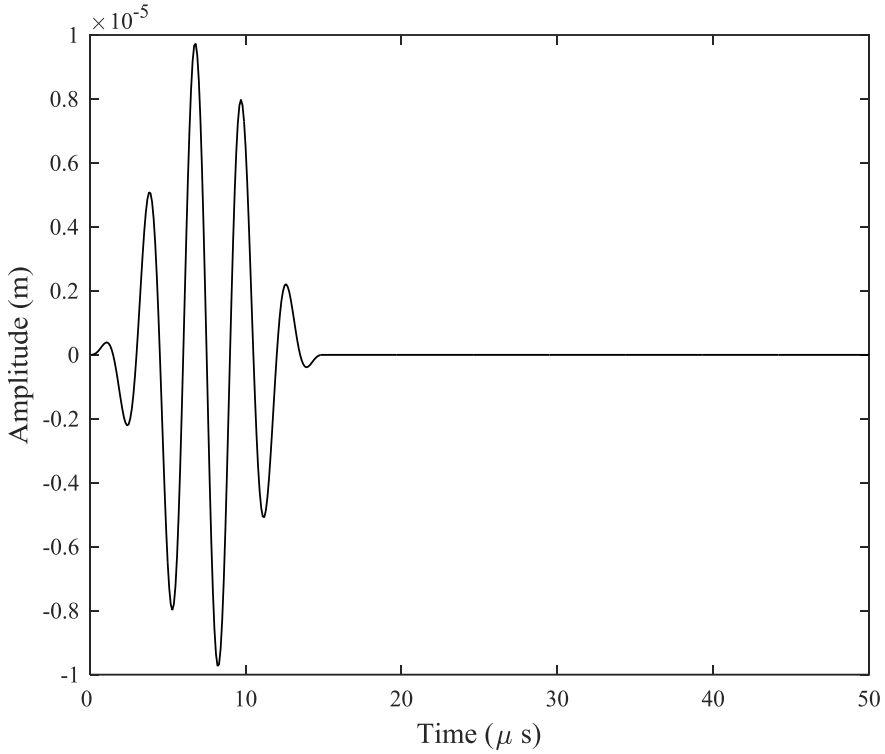

(a) Lamb wave

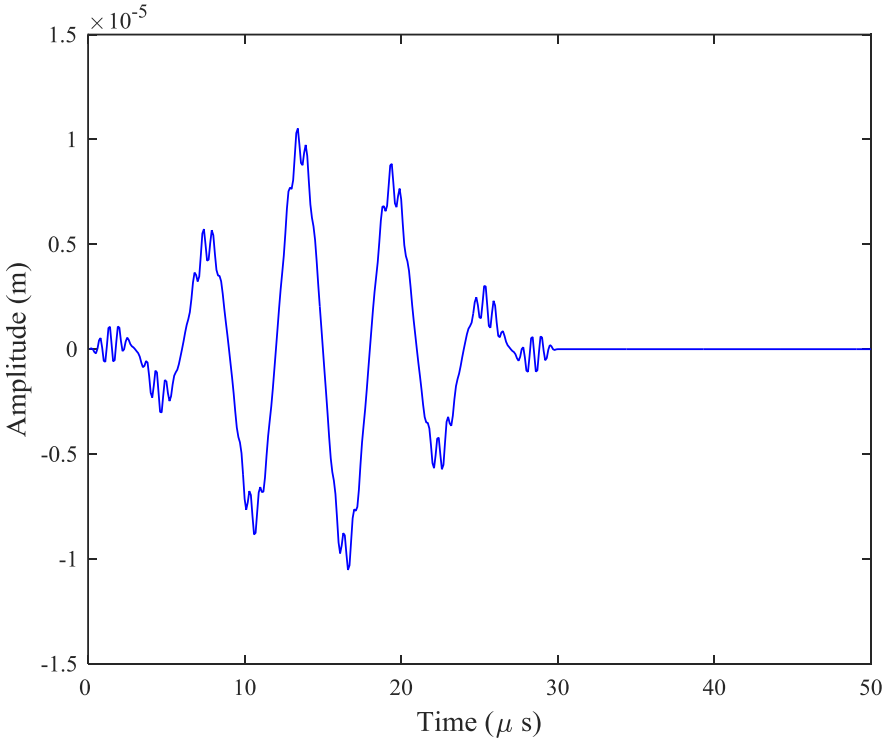

(b) Lamb wave with higher harmonics

Figure 3.11. Excitation signal

The excitation signal on a plate with a higher harmonics is shown in Figure 3.11(b). An Al plate of 500 mm length and 1 mm thickness is considered as second example in the analysis. The material properties are assumed as Poisson's ratio=0.3, density=2700 Kg/m^3, and Young's modulus E=69 GPa. The Lamb wave in this material has longitudinal velocity C_L = 5299 m/s and transverse velocity C_T = 3135 m/s. The waves are actuated by employing pin forces applied to the left boundary of the plate. The excitation forces are perpendicular to the longitudinal (propagating) direction. In-phase pin forces are applied to the top and bottom edge nodes of the plate for excitation of fundamental symmetric (S_0) modes, and the anti-symmetric modes are propagated by imposing out-of-phase pin forces. In this paper, we considered a case in which the pure S_0 mode is excited. To provide a limited cycle sinusoidal tone burst, five cycles Hanning-window excitation signal is applied.

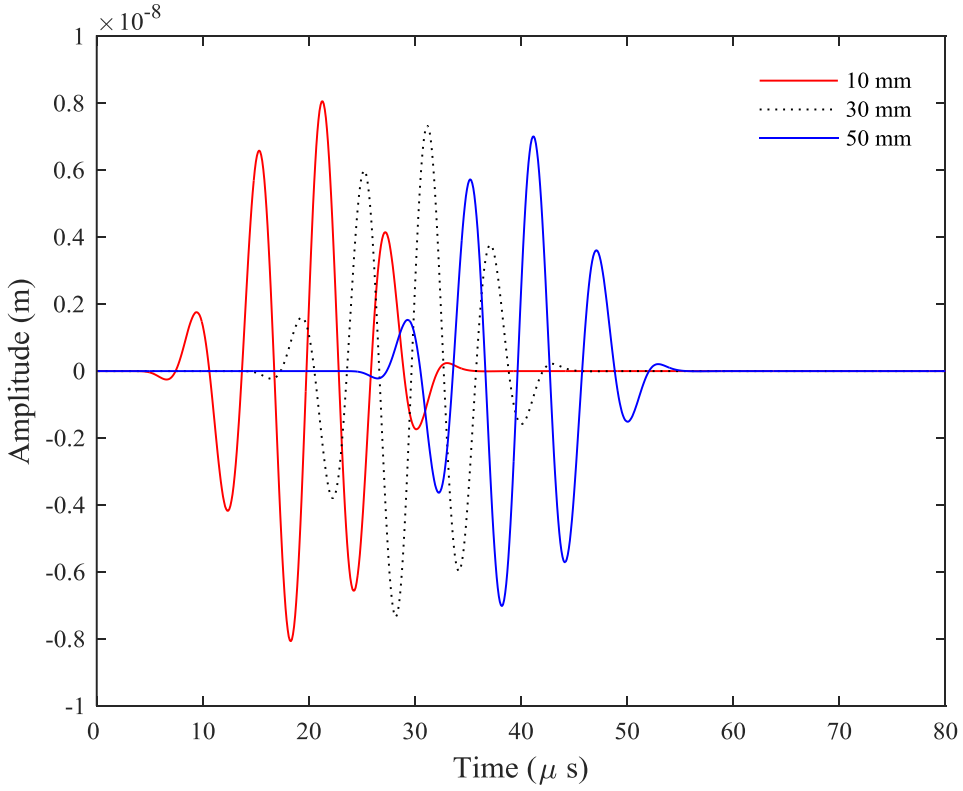

Figure 3.12. Wave propagation for 400 kHz center frequency in plate at different nodes

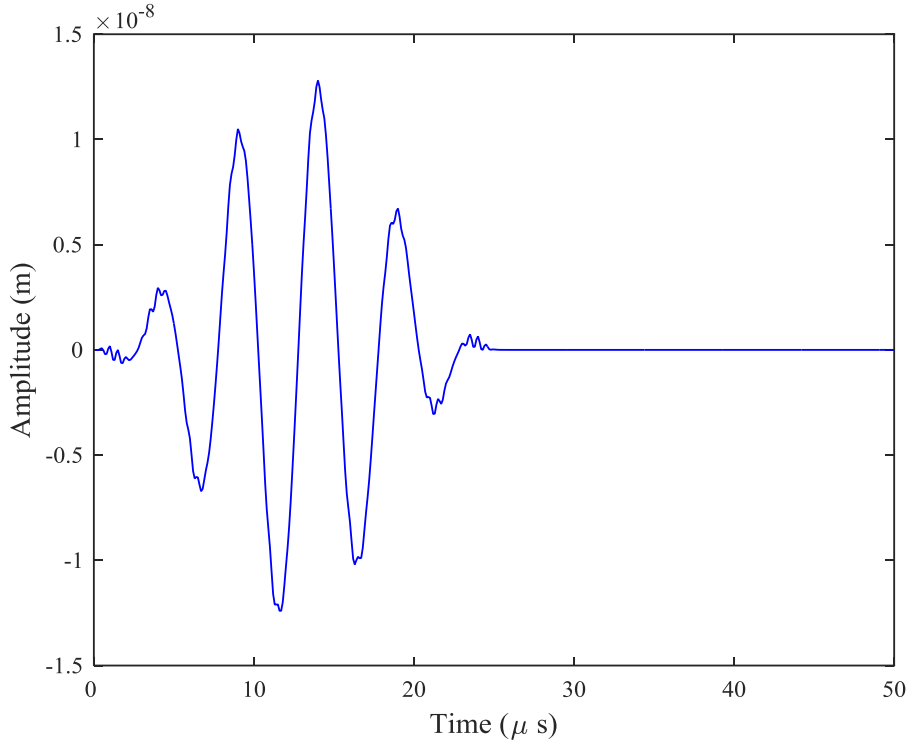

(a) 50 elements per wavelength

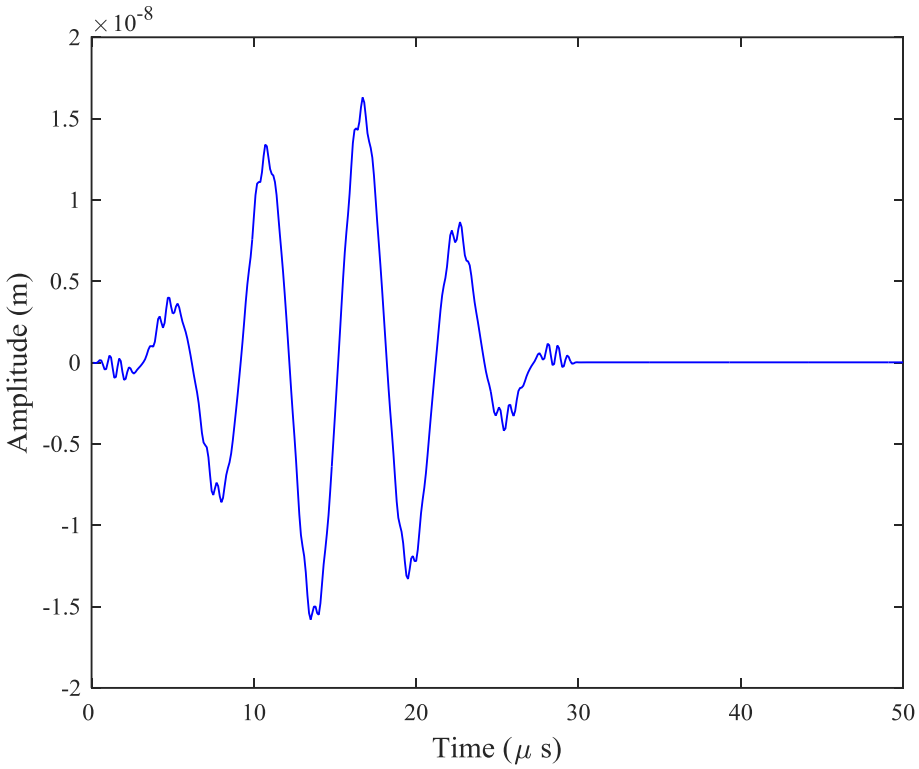

(b) 100 elements per wavelength

Figure 3.13. Response of plate with no. of elements per wavelength

Lamb wave propagation signals on a plate at different nodes at the distance of 10, 30 and 50 mm from the left end, generated by FEM, are illustrated in Figure 3.12. It can be observed that wave is propagated but there is some dispersion. Generally, 20 elements per wavelength are required in the case of Lamb wave, but this is not sufficient for higher harmonic simulation. Higher frequency wave propagation problems demand enormous computer resources because of highly dense mesh and very large number of time integration steps. Figure 3.13(a) depicts the measured nodal displacement response of time-domain signals obtained using FEM simulation of the plate with 50 elements per wavelength. It can be observed that higher harmonics are not properly visible. On the other hand, as shown in Figure 3.13(b), higher harmonics are visible for 100 elements per wavelength.

In the present analysis, B-spline and Daubechies (D4) wavelet are used to establish robustness and sensitivity of wavelet based wave propagation method. To capture higher harmonics in the plates, FEM uses 17080 uniformly distributed nodes while half of the FEM nodes are required after application of one level of wavelet transform. Nodal displacement response of plate received from B-spline and D4 wavelet Transform at level 1 along with FEM results are demonstrated in Figure 3.14. It establishes a good agreement between conventional finite element and proposed wavelet-based method. It can be observed that B-spline wavelet produces response close to FEM results, while there is some deviation in the results of D4 wavelet.

Further we examined wavelet-based method at the various level of wavelet transform to find the level up to which this method can work efficiently. In next wavelet transform level, the number of uniformly distributed nodes are reduced to 4270 which is one-fourth of the FEM nodes and the results are shown in Figure 3.15. Similarly, wavelet

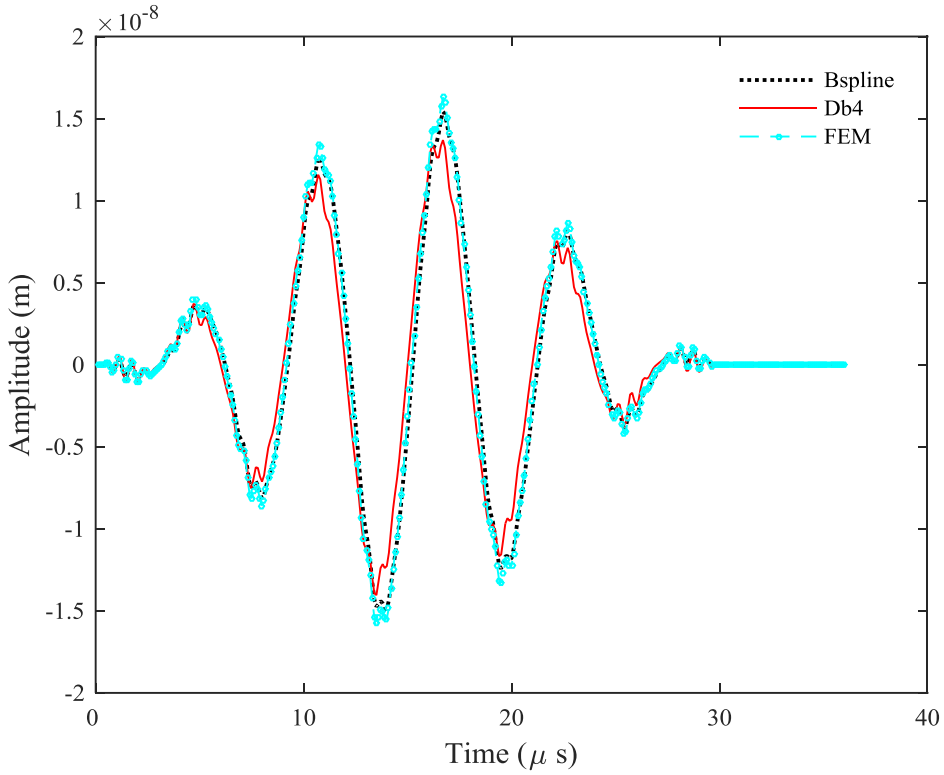

Figure 3. 14. Comparison of plate response at wavelet transform level 1

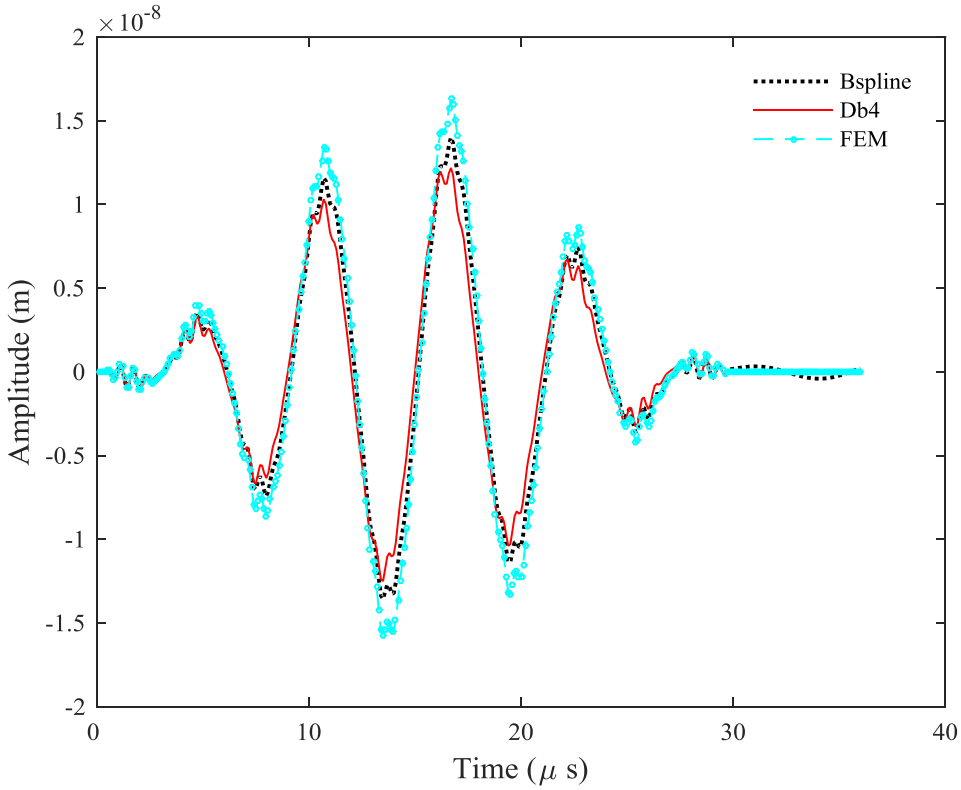

Figure 3. 15. Comparison of plate response at wavelet transform level 2

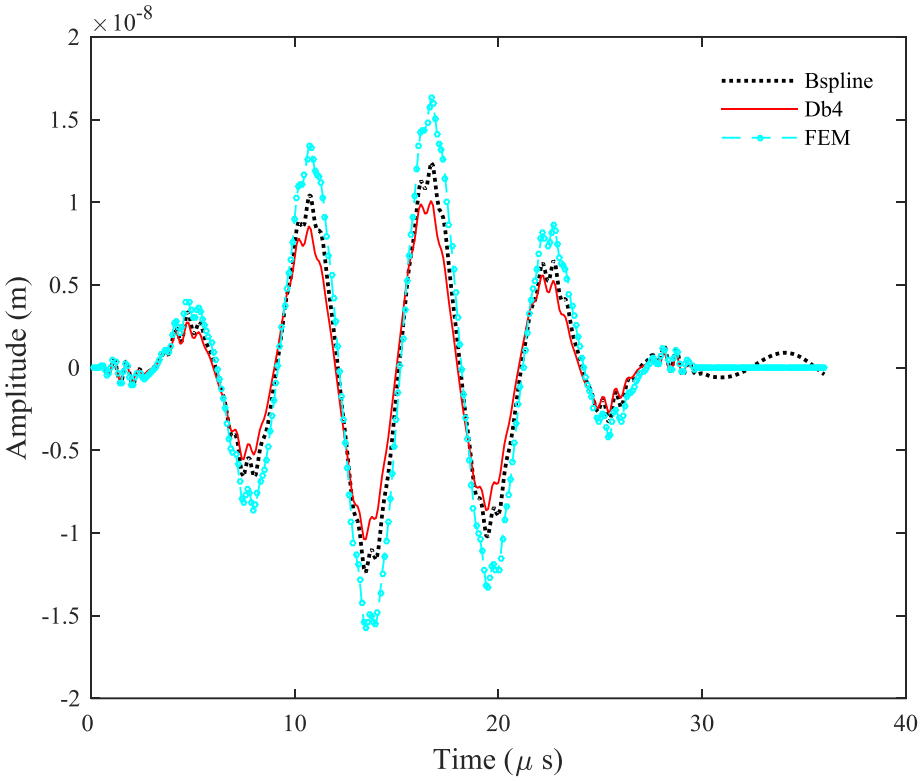

Figure 3. 16. Comparison of plate response at wavelet transform level 3

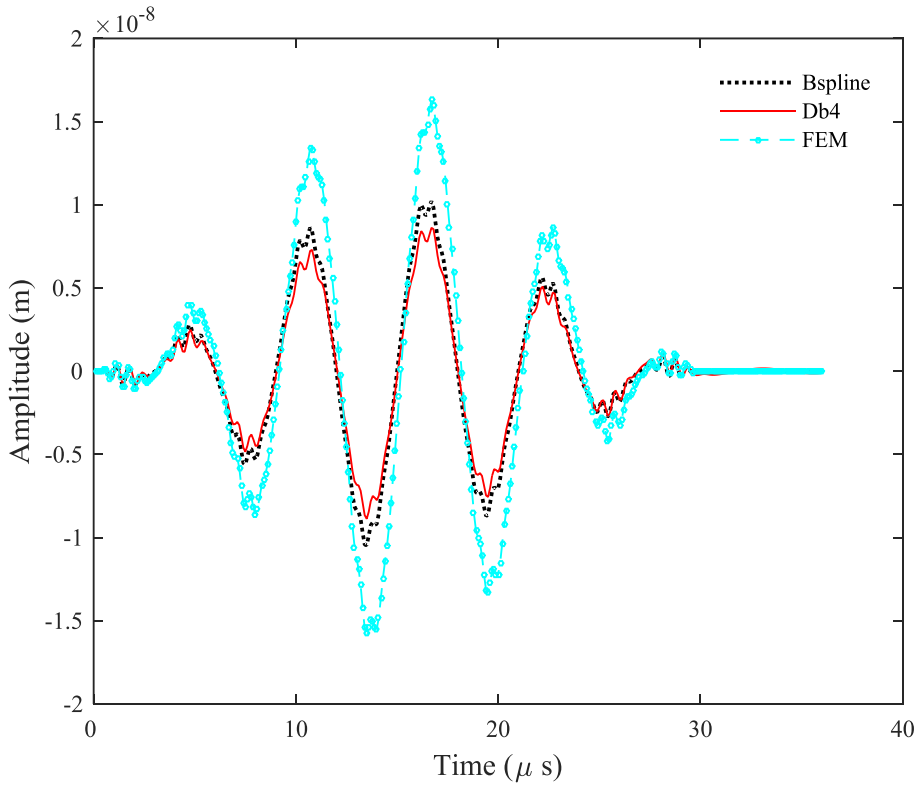

Figure 3. 17. Comparison of plate response at wavelet transform level 4

transform level-3 is utilizing only 2135, i.e. one-eighth of the FEM nodes. The resulting wavelet response and FEM response of the plate are shown in Figure 3.16. These results show some attenuation but wavelets are not eliminating higher frequency components of waves which are important in many analyses. Wavelet transform level-4 uses only 1068 nodes which is one-sixteenth of the FEM nodes. As shown in Figure 3.17, such a small number of nodes are also sufficient to observe higher harmonics. It is evident as low as 6.25 % of FEM nodes is sufficient to propagate higher harmonics in the plates when proposed wavelet based is used. The numerical results confirm the multiresolution properties of the wavelet based method, which reveals that the proposed technique are effective.

The proposed scheme presents computationally less expensive solution due to the multiresolution capability of wavelets. This property suggests that one could approach the problem by initially computing the coarse scale wavelet coefficients of the solution, and then incrementally refining the solution by computing the finer scale wavelet coefficients. To be efficient, a multiscale solver should progress from one resolution to the next by performing a minimal amount of additional work, i.e. the computation of a finer scale solution from a previously computed coarser scale solution. The computation of the solution is terminated as soon as an acceptable accuracy is achieved.